Accepted Manuscript

One pot synthesis of TiO_2: Eu^{3+} hierarchical structures as a highly specific luminescent sensing probe for visualization of latent fingerprints

K.R. Venkatesha Babu, C.G. Renuka, R.B. Basavaraj, G.P. Darshan, H. Nagabhushana

Please cite this article as: Babu KRV, Renuka CG, Basavaraj RB, Darshan GP, Nagabhushana H, One pot synthesis of TiO_2: Eu^{3+} hierarchical structures as a highly specific luminescent sensing probe for visualization of latent fingerprints, *Journal of Rare Earths* (2018), doi: 10.1016/j.jre.2018.05.019.

This is a PDF file of an unedited manuscript that has been accepted for publication. As a service to our customers we are providing this early version of the manuscript. The manuscript will undergo copyediting, typesetting, and review of the resulting proof before it is published in its final form. Please note that during the production process errors may be discovered which could affect the content, and all legal disclaimers that apply to the journal pertain.

One pot synthesis of TiO$_2$: Eu^{3+} hierarchical structures as a highly specific luminescent sensing probe for visualization of latent fingerprints

K.R. Venkatesha Babu[1, 2], C.G. Renuka[1,*], R.B. Basavaraj[3], G.P. Darshan[4], H. Nagabhushana[3, *]

[1]*Department of Physics, JnanaBharathi Campus, Bangalore University, Bangalore-560 056, India*
[2]*Department of Physics, Govt. Science College, Bengaluru-560 001, India*
[3]*Prof. C.N.R. Rao Centre for Advanced Materials, Tumakuru University, Tumakuru-572103, India*
[4]*Department of Physics, Acharya Institute of Graduate Studies, Bangalore 560 107, India*

Abstract

In the present work, TiO$_2$:Eu^{3+} (1 mol%–11 mol%) nano powders (NPs) were prepared via a facile one-pot hydrothermal method by using *Epigallocatechin Gallate* (EGCG) as bio-surfactant. The optimized TiO$_2$:Eu^{3+} (5 mol%) NPscan be used as fluorescent labeling agent for visualizing of latent fingerprints (LFPs) on various porous and non-porous surfaces. The obtained results exhibit well defined ridge details with high sensitivity, selectivity, and low background hindrance which show greater advantages as compared to conventional powders. We demonstrate the viability of high-performance security labels thorough excellent luminescence for practical anti-mimetic applications. Morphology of the prepared samples were highly dependent on pH, concentration of the bio-surfactant, temperature and time durations. Photoluminescence (PL) emission spectra exhibit intense red emission at ~ 615 nm due to electric dipole transition ($^5D_0 \rightarrow {}^7F_2$). Photometric (CIE and CCT) results clearly show the intense warm red emission of the optimized samples. Therefore, this work offers a superior and universal luminescent label, which can be applied to visualize miniature LFPs particulars for individualization and consequently display great prospective in forensic investigation.

*Corresponding Author: C. G. Renuka (Email: renubub@gmail.com; Tel: +91- 9844106025); H. Nagabhushana (E-mail: bhushanvlc@gmail.com; Tel: +91-966-3177440).

1. Introduction

Currently, the focus of nanoscience was gradually shifting towards the synthesis of organized hierarchical nanostructures with precise size and shape to overcome the drawbacks of individual nanoparticles in various fields, such as nanophotonics, metamaterials, and biotechnology [1-3]. Owing to their collective behaviour, the hierarchical nanostructures exhibit smart functions, including better luminescent properties than those of bulk and individual nanomaterials. Based on these advantages, we focused on the development of crystal-splitting-induced novel fluorescent hierarchical nanostructures with desirable size and shape for improved, simultaneous identification at three levels from LFPs imaging by staining with the synthesized hierarchical structures [4-6].

Fluorescence materials were known for their use in solid state lighting, biomedical labeling and thermometry [7-10]. Despite their wide application, these materials were still researched in latent fingerprint detection of forensic science. Fingerprints (FPs)were one of the physical evidence to identify personal information owing to permanent information about each person. Owing to these properties, recovery and detection of fingerprint was an important process in forensic science. In particular, reveal and identification of invisible fingerprints (called LFPs) can be a contribution to suspect the crime scene. The fingerprinting powder which was categorized according to its composition and properties is regular, metallic and luminescent powders [11-13]. The regular fingerprint powder was combined with adhesive polymer and dye material. Metallic fingerprint powder was the meshed metal particle, such as gold, silver. Although the regular and metallic fingerprint powder were simple and easy to used, both powder has problems with their low contrast, low sensitivity, high background interference and high toxicity [14,15].

FPswere typically not visible to the naked eye; thus, one or several appropriate physical or chemical techniques were required for detection and visualization, including powder dusting, fluorescent dye staining, cyanoacrylate/iodine fuming, and vacuum metal deposition, etc. [16-19]. Visualization was possible because FPs contain a variable mixture of water, fatty acids, salts, free amino acids, etc. The methods via the interaction with these components, especially the selective attack of the amino acids or fatty residues, provide some contrast between the surface and fingerprint ridges, leading to the enhancement of LFPs [20]. Among various detection techniques, fluorescence staining was a general method for the detection of LFPs with high sensitivity.

Titanium dioxide (TiO_2) creates considerable attention for the research community due to its chemical and thermal stability, wide band gap, and nontoxic nature [21-25]. Its outstanding properties find many industrial applications, namely, cosmetics products, decorates, and coloring agent in consumable foods [26-28].In addition, TiO_2 is considered as novel photoactive material and hence it was used as a photo catalyst for ecological conservation, namely degradation of water as well as air pollutants and production of sustainable energy (hydrogen generation). The RE modified TiO_2 exhibits tremendous applications as phosphor material. However, there was still a task for the research community to improve effective synthesis protocol for the preparation of well crystalline RE modified TiO_2powders because ionic radii mismatch between dopants and Ti^{4+} site [29, 30].

Herein, we report a simple hydrothermal method to synthesize the novel red light emitting $TiO_2:Eu^{3+}$ (1 mol%–11 mol%) NPs using EGCG as surfactant. The effect of surfactant concentration, pH, temperature and reaction time on the morphology and photoluminescence was studied in detail. The optimized NPs were used to visualize LFPs on various porous, and non-porous surfaces. The security characters by general dip-pen technique using the transparent security ink prepared using optimized NPswere demonstrated.

2. Materials and methods

Novel $TiO_2:Eu^{3+}$ (1 mol%–11 mol%) NPs were fabricated by a facile one-pot hydrothermal route by using EGCG as bio-surfactant. The procedure for preparation of EGCG extraction was described elsewhere [31]. The stoichiometric quantities of titanium (IV) isopropoxide $Ti[OCH(CH_3)_2]_4$, europium(III) nitrate pentahydrate ($Eu(NO_3)_3 \cdot 5H_2O$) and 20 mL ethanol were placed in a beaker and stirred thoroughly with magnetic stirring for ~10 min. Later, 5 and 15 mL of EGCG and ethanol were added to the resultant precursor solution and then transferred to a 80 mL Teflon-lined autoclave maintained at ~100 °C for 6 h time duration. The obtained samples were washed with distilled water and ethanol for several times. The obtained final sample was further annealed at ~600 °C for ~3 h. The sample preparation was continual by changing Eu^{3+} concentration, pH level of the solution, EGCG concentration, reaction time duration and temperature. Fig.1 shows the pictorial illustration of extraction of EGCG, hydrothermal synthesis of Eu^{3+} doped TiO_2 NPs and its applications.

2.2. Instruments used

AShimadzu made powder X-ray diffractometer (PXRD, 7000) with nickel filter was used to obtain diffraction data to study phase purity and crystallinity of the samples. Scanning electron microscopy (SEM, Hitachi 3000) and transmission electron microscopy (TEM, Hitachi H-8100 accelerating voltage up to 200 kV) were used to study the morphology of the

samples. The Raman studies were recorded through Jobin YVON Horiba LABRAM-HR-visible micro Raman system with He-Ne laser (~632.8 nm) as the source. The photoluminescence (PL) data were recorded using a Jobin YVONSpectrofluorimeter with 450 W Xenon lamp as an excitation source.

2.3. Visualization of LFPs using optimized TiO$_2$:Eu^{3+} (5 mol%) NPs

The LFPs on various porous and non-porous surfaces were collected from different donor. Before pressing against substrate surface, the hands of the donors were thoroughly washed with the soap and gently wiped across the ridges. After that, the fingertip of volunteer was rubbed over their forehead or nose region, and randomly pressed on the substrates. Then, the synthesized TiO$_2$:Eu^{3+} (5 mol%) NPs were stained on the impressed LFPs by a soft feather brush with light brushing action. Finally, the developed LFPs were photographed under 254 nm UV lamp using DSLR Canon EOS 100D camera with 5 mm lens (SIGMA MACRO, 50 mm, F2.8, EXDG).

3. Results and discussion

3.1. X-ray diffraction analysis

Fig. 2(a)shows the PXRD results of both pure and TiO$_2$:Eu^{3+} (1 mol%–11 mol%) NPs. The obtained profiles werewell matched to pure anatase phase of TiO$_2$ with standard JCPDS card no.21-1272[32]. No other impurity and Eu^{3+} ions peaks were observed in the profiles, indicating that dopant Eu^{3+} ions were effectively substituted in the Ti^{4+} site in the TiO$_2$ host. In the present work, the value D_r between Ti^{4+} and Eu^{3+} ion was estimated by using the following relation[33]:

$$D_r = \frac{R_s - R_d}{R_s} \text{---------------- (1)}$$

where, R_s and R$_d$; ionic radii doped Eu^{3+} ion (0.1066 nm) and substituted Ti^{4+} site (0.074 nm), respectively. The value of D_r was estimated and obtained to be ~30%, indicating that dopant Eu^{3+} ions were effectively substituted to Ti^{4+} sites in TiO$_2$ host.

The diffraction peaks broadening were commonly connected with crystallite size or the lattice strain present within the sample or both. Scherrer's relation [34] was utilized to determine the average crystallite size of the prepared NPs, as given below:

$$D = \frac{0.9\,\lambda}{\beta \cos \theta} \text{------------------ (2)}$$

where β represents full width at half maxima (FWHM) in radian, λ X-ray wavelength (0.1542 nm), θ the Bragg's angle. The D values of the prepared samples were estimated and given in Table 1. Further, the crystallite size and the micro strain present in the NPs were also calculated using Williamsons-Hall (W-H) plots[35]:

$$\frac{\beta \cos \theta}{\lambda} = \frac{1}{D} + \frac{\varepsilon \sin \theta}{\lambda}$$ ------------ (3)

where D denotes crystallite size, λ; wavelength of Cu Kα radiation, β FWHM of peak, and θ Bragg's diffraction angle. The W-H plot is shown in Fig. 2(b).The obtained results are given in Table 1 and it is evident that with increase of Eu^{3+}ion concentration the crystallite size decreases and strain increases.

3.2. Morphological analysis

Fig.3 shows SEM images of the hydrothermally synthesized TiO$_2$:Eu^{3+} (5 mol%) hierarchical structures prepared by various concentrations of EGCG bio-surfactant (5–30 mL). It was observed that obtained structures were mainly depending on the concentration of EGCG. Fig. 3(a) depicts SEM images of the samples prepared in the presence of EGCG concentration (5 mL). The obtained result exhibits individual and irregular mushroom shaped particles. Further, when the concentration of bio-surfactant EGCG concentration was increased to 10–20 mL, individual particles undergo self-assembly in an oriented direction to form stem-like structures (Fig. 3(b–d)). Bio-surfactant EGCG allows the axial growth of initial structures, due to its strong chelating and excellent capping capabilities. In addition, with increasing the 25 and 30 mL EGCG concentration, densification occurs with the formation of uniform self-organization and surface smooth of stem like structures giving rise to hierarchical architectures (Fig. 3(e, f)).

The morphology of the TiO$_2$:Eu^{3+} (5 mol%) NPs is strongly influenced by varying pH value of the solution with fixed EGCG concentration (20 mL), as shown in Fig. 4. Initially the pH level of the reaction solution was 1 and 3, the product exhibits uniform and is entirely composed of dumbbell shaped microstructures (Fig. 4 (a, b)). When the pH of the solution was increased to 5 and 9, the dumbbells shaped subunit have a high surface energy and an affinity to aggregate, thus reducing this energy and achieving thermodynamic stability via self-assembly and formation of hierarchical flower-like architecture (Fig. 4(c & d)).

Fig. 5 shows the advancement during formation of hierarchical flower- like structures prepared by hydrothermal route with different time period (6–24 h), fixed EGCG

concentration (20 mL) and pH = 3. During the initial stage of 6 and 12 h, the product is composed of many irregular particles (Fig. 5(a, b)). When the hydrothermal treatment was extended to 18 h, irregular particles undergo growth and oriented attachment to form flattened flower-like structure. With increasing the reaction time to 24 h, uniform and homogeneous flower-like microstructures were obtained (Fig. 5(d)).

SEM images of the hydrothermally synthesized $TiO_2:Eu^{3+}$ (5 mol%) hierarchical structures prepared by various temperatures (100–140 ℃) with fixed EGCG concentration (20 mL), pH 3 and time duration of 12 h are shown in Fig. 6. Initially at 100 °C, un-ripened flower like architecture was observed. The obtained flower like hierarchical architecture formed via self-assembly of 2D nano sheets as building blocks. Further, hydrothermal temperature was maintained at 140 °C, resulted in modification of the original shape: well developed micro-flower like structures was observed.

Based on the obtained results, a tentative mechanism for the formation of various NPs is proposed (Fig. S1). Initially, when the EGCG concentration is added to the precursor solution, the EGCG reacts with the Ti^{4+} and Eu^{3+} viastrong chelating interaction and forms hierarchical NPs. During growth stage, EGCG selectively adsorbs on the facets of nucleates and controls their growth in an oriented direction. These oriented subunits have a high surface energy and a tendency to aggregate, thus reducing this energy and achieving thermodynamic stability via self-assembly and leading to the hierarchical NPs.

TEM image of the optimized $TiO_2:Eu^{3+}$ (5 mol%) NPs is shown in Fig. 7(a). A smooth uniform nano flower-like architectures was observed. From HRTEM image, interplanar spacing (*d*) between lattice planes was measured and found to be ~0.27 and 0.31 nm for (101) plane of $TiO_2:Eu^{3+}$ (5 mol%) NPs, is shown in Fig. 7(b, c). The SAED patterns show that the samples were well-crystallized and were consistent with the PXRD analysis. Further, discontinuous ring patterns along with sharp spots indicate the presence of nano-sized particles (Fig. 7(d)).

3.3. Raman spectroscopic analysis

Fig. S2 shows the Raman spectra of $TiO_2:Eu^{3+}$ (1 mol%–11 mol%) NPs calcined for 600 °C for 3 h. The Raman bands observed at ~ 142 (E_g), 395 (A_{1g}), 513.46 (B_{1g}) and 639.18 cm^{-1} (E_g) are attributed to Raman active modes of anatase phase of TiO_2 [36, 37].The small shift in the highest peak (~142 cm^{-1}) may be due to creation of oxygen vacancies caused by the charge difference between Eu^{3+} and Ti^{4+}. The mode at ~142 and 513.46 cm^{-1} was mainly ascribed to symmetric stretching vibration and bending vibration of O–Ti–O, respectively.

However, mode at 395 cm^{-1} was due to the anti-symmetric bending vibration of O–Ti–O. No characteristic peaks of Eu$_2$O$_3$ or EuO were observed in the Raman spectra, which clearly establish formation of Eu$_2$Ti$_2$O$_7$ phase[38].

3.4. Photoluminescence studies

The PL excitation spectrum of TiO$_2$:Eu^{3+} (5 mol%) NPs recorded at λ_{em}= 615 nm is shown in Fig. 8(a). The spectrum consisted of several sharp peaks at ~362, 384, 395, 416, and 462 nm, which were attributed to $^7F_0 \rightarrow {}^5L_6$, $^7F_0 \rightarrow {}^5D_4$, $^7F_0 \rightarrow {}^5L_7$, $^7F_0 \rightarrow {}^5D_3$, and $^7F_0 \rightarrow {}^5D_2$ transitions, respectively[39]. Fig. 8(b) shows the PL emission spectra of Eu^{3+} (1 mol%–11 mol%) doped TiO$_2$ NPs recorded by exciting at 395 nm wavelength. The spectra exhibit intense peaks at ~ 580, 612, 652 and 703 nm, which were ascribed to $^5D_0 \rightarrow {}^7F_0$; $^5D_0 \rightarrow {}^7F_2$, $^5D_0 \rightarrow {}^7F_3$ and $^5D_0 \rightarrow {}^7F_4$ transitions of Eu^{3+} ions, respectively[40]. The intense peaks at 580 and 612 nm were belong to magnetic dipole and forced electric dipoletransitions, respectively. When the dopant Eu^{3+} ions concentration increases, the luminescence intensity increases up to 5 mol% and then diminishes due to concentration quenching phenomena (Inset: Fig. 8(b)). The concentration quenching may be attributed to decrease of resonant energy transfer rate between the donor to acceptor ions in the host lattice. The energy transfer mechanism can be explained using the critical distance (R_c) between the Eu^{3+} ions as given below[41]:

$$R_c = 2 \left[\frac{3V}{4\pi X_c Z} \right]^{1/3} \text{-------------- (2)}$$

where X_c denotes critical concentration (0.05), Z number of cation sites in the unit cell (6), and V volume of the unit cell (13.584 nm). The estimated value of R_c was found to be 0.952 nm, which was greater than 0.5 nm suggesting that the multipole–multipole interaction is a major cause of concentration quenching phenomena.

In addition, the effect of various reaction parameters namely, EGCG concentration, pH of the precursor solution, heating rate and time duration on the PL emission was also studied in detail. No obvious change in the emission profile, while variation in the intensity of the peaks was observed in all the cases. Fig. 8(c) shows the variation of PL intensity of TiO$_2$:Eu^{3+} (5 mol%) with respect to EGCG concentration. It was observed that the maximum emission intensity was observed for 20 mL of EGCG concentration (Inset: Fig. 8(c)). Hence, the surfactant EGCG concentration is optimized to be ~ 20 mL. Further, the pH value of the precursor solution and heating rate were varied by fixing EGCG concentration to ~ 20 mL (Fig. 8(d, e)). It was observed from the figure that the maximum emission intensity was observed for pH = 3 and 120 ^{o}C for 12 h. Further, effect of hydrothermal reaction duration (6

– 24 h) on the PL emission was studied by fixing optimized experimental conditions (Fig. 8(f)). It was evident from the figure that the emission intensity was almost 2-fold enhanced and maximum intensity was observed for 12 h hydrothermal reaction.

The luminescence color of the prepared samples was estimated by using the emission intensity and corresponding wavelengths. It was noticed that the estimated CIE coordinate values were situated in the red region of the chromaticity diagram. Further, correlated color temperature (CCT) values were also estimated using standard relation described elsewhere [42]. The corresponding CIE and CCT diagrams are given in (Fig. 9 (a, b)). The average CCT value for the present phosphor was found to be ~ 2509 K, which corresponds to warm LEDs.

3.5. Fingerprint analysis

LFPs residues mainly contain moisture such as sweat from eccrine glands and oily constituents namely, grease and oil from sebaceous glands. Thus, powder dusting was typically physical method that relies on the adsorption capacity of FP powder to the moistures and oily constituents [43]. To assure a high contrast for the development of the FPs, both a high luminescent intensity and a low amount of background interference were highly required. To achieve a high resolution image for development, the particle size must be in nano size. To obtain a better selectivity between powders and papillary ridges, a uniform size was required for suitable adsorption capacity [44]. The novel developing strategy set up by our use of (5 mol%) NPs as fluorescent powders was straightforward, rapid, and efficient that it primarily needed a soft feather brush instead of the commonly used squirrel brush.

3.5.1 Visualization of LFP on porous surfaces

The concept of contrast in LFP visualization means the comparison between the papillary ridges of the fingermark and the background of the substrates, similar to a signal to noise ratio in analytical chemistry. Hence, enhancing the signal and lowering the background noise were suggested as two approaches for ensuring high contrast. To prove the high contrast of the $TiO_2:Eu^{3+}$ when used for fingermark development, multicolored magazine cover was selected as the smooth surface and stained with optimized $TiO_2:Eu^{3+}$ (5 mol%) NPs via powder staining route (Fig. 10). The results indicated that the substrate surface did not affect the interaction between $TiO_2:Eu^{3+}$ NPs with the FPs.

3.5.2 Visualization of LFP on non-porous surfaces

Further, to confirm the practical applicability of optimized $TiO_2: Eu^{3+}$ (5 mol%) NPs for LFPs visualization on various non-porous surfaces namely, mouse, metallic scale and scissor were used and are shown in Fig. 11(a–c). Well defined FPs with three level details were clearly revealed on all surfaces, indicating that optimized sample quite effective for the

visualization of LFPs without any background hindrance. Therefore, optimized phosphors can have great potential application for visualization LFPs.

In LFPs visualization, selectivity refers to the specific adherence of the developing reagents to papillary ridges, rather than to the furrows of the background. The pixel profile of the images at higher resolution indicated both the raised ridges and the furrows were stained using optimized NPs (Fig. 11(d)). The papillary ridges of this developed FPs appeared to be fuzzy, showing the low selectivity. By using $TiO_2:Eu^{3+}$ (5 mol%) as fluorescent labels, the FPs exhibited sharp and well-defined papillary ridges, almost without any background stains. The results revealed that the optimized NPs were present on the ridges rather than in furrows. Thus, we could ascribe the high selectivity of optimized powder as a fluorescent label for FPs visualization due to the uniform particle size. Furthermore, it was also worth mentioning that our method was so quick, efficient and completed within 30 s after moderate training. Therefore, these results confirmed that the $TiO_2:Eu^{3+}$ (5 mol%) NPs were a potential and valuable candidate for the powder dusting method for visualization of LFPs on various substrates.

3.5.3 Visualization of various donor LFPs and ridge details using optimized powder

Further, various donors FPs were visualized by optimized NPs on aluminum foil surface as shown in Fig. 12. The obtained result clearly shows four different level 1 details namely, central pocket whorl, plain whorl, arch and loop, indicating that FPs were unique for all the individuals. To visualize the LFPs is in fact to provide the informative properties of the papillary ridges of the LFPs, and these pieces of information can be classified into three levels. Level 1 provides the pattern information (arches, loops, whorls, and compounds) of LFPs. Level 2 describes the minutia points including core, bifurcation, delta, bridge, enclosure, island, short ridge, and hook, and their random combinations endow the uniqueness and invariability of FPs. In addition, level 3 refers to the shape, number, and location of sweat pores, and although they alone cannot be used to detect LFPs, they provide reference information for partial defect or blurry level 2 of LFPs. As shown in Fig. 13, the level 1 detail (whorl ridge pattern) and more comprehensive details of level 2 could be easily recognized by naked eyes. Furthermore, the level 3 information (sweat pores) can also be obtained, which was highly desired for individual identification. These excellent optical behaviors not only were sufficient for individualization but also can be used for exclusion, which were crucial for forensic investigations by circumventing issues related to sufficient contrast between the background and FP ridges arising from multicolored surfaces. Take the fluorescent images under UV wavelength for example, the ridge pattern details of LFPs on

aluminum foil surface could be clearly identified by bare eyes, which would provide sufficient evidence for individual identification (see in Fig. 13).

Non-destructive methods for collecting evidence were significant in the field of forensics. Due to the geometry of the substrates, non-destructive imagining of FPs on bent surfaces remains challenging. The powder dusting method was used for visualizing and recording FP arrays on non-porous curved surfaces, including soft drink can, stainless steel spoon, spray bottleandbar code on chemical bottle (Fig.14). Clear FP patterns were visualized without further processing to enhance the contrast between the FP area and background.

4. Conclusions

In summary, a facile synthesis of $TiO_2:Eu^{3+}$ (1 mol%–11 mol%)NPs were designed via a one-pot hydrothermal route. The morphological results show that the resultant powders possess various hierarchical structures as a function of different reaction parameters. Furthermore, well-defined papillary ridges with enhanced contrast, higher sensitivity, and better selectivity when compared with conventional developing methods, suggest that the optimized sample was explored as a novel labeling agent for visualization of LFPs. The spectra exhibit intense peaks at ~ 580, 612, 652 and 703 nm, which are ascribed to $^5D_0 \rightarrow {^7F_0}$; $^5D_0 \rightarrow {^7F_2}$, $^5D_0 \rightarrow {^7F_3}$ and $^5D_0 \rightarrow {^7F_4}$ transitions of Eu^{3+} ions, respectively. The Raman spectra show bands at ~ 142 (E_g), 395 (A_{1g}), 513.46 (B_{1g}) and 639.18 cm^{-1} (E_g) attributed to Raman active modes of anatase phase of TiO_2. Optimized$TiO_2:Eu^{3+}$ (5 mol%) NPs are quite useful in advanced forensic applications.

References

1. Basavaraj RB, Nagabhushana H, Daruka Prasad B, Vijayakumar GR. Zinc silicates with tunable morphology by surfactant assisted sonochemical route suitable for NUV excitable white light emitting diodes. Ultrason. Sonochem. 2017;34:700.
2. Suresh C, Nagabhushana H, Darshan GP, Basavaraj RB, Daruka Prasad B, Sharma SC, *et al.* Lanthanum oxyfluoride nanostructures prepared by modified sonochemical method and their use in the fields of optoelectronics and biotechnology. Arab J Chem.2018;11:196.
3. Song WL, Zhou ZL, Wang LC, Cheng XD, Chen MJ, He RJ, *et al.* Constructing repairable meta-structures of ultra-broad-band electromagnetic absorption from three-dimensional printed patterned shells. ACS Appl Mater Interfaces. 2017;9:43179.
4. Basavaraj RB, Nagabhushana H, Darshan GP, Daruka Prasad B, Sharma SC, Venkatachalaiah KN. Ultrasound assisted rare earth doped Wollastonite nanopowders: labeling agent for imaging eccrine latent fingerprints and cheiloscopy applications. J Ind Eng Chem. 2017;51:90.

5.   Basavaraj RB, Nagabhushana H, Darshan GP, Daruka Prasad B, Rahul M, Sharma SC, *et al.* Red and green emitting CTAB assisted $CdSiO_3:Tb^{3+}/Eu^{3+}$ nanopowders as fluorescent labeling agents used in forensic and display applications. Dyes Pigm. 2017;147:364.

6.   Marappa B, Rudresha MS, Basavaraj RB, Darshan GP, Daruka Prasad B, Sharma SC, *et al.* EGCG assisted $Y_2O_3:Eu^{3+}$ nanopowders with 3D micro-architecture assemblies useful for latent finger print recognition and anti-counterfeiting applications. Sens Actuators B. 2018;264:426.

7.   Basavaraj RB, Darshan GP, Daruka Prasad B, Sharma SC, PaneerSelvam, Premkumar, *et al.* Rapid visualization of latent fingerprints using novel $CaSiO_3:Sm^{3+}$ nanophosphors fabricated via ultrasound route. J Rare Earths. (Accepted 2018).

8.   Venkatachalaiah KN, Nagabhushana H, Basavaraj RB, Darshan GP, Daruka Prasad B, Sharma SC. Flux blended synthesis of novel $Y_2O_3:Eu^{3+}$ sensing arrays for highly sensitive dual mode detection of LFPs on versatile surfaces. J Rare Earths. (Accepted2018).

9.   Venkataravanappa M, Basavaraj RB, Darshan GP, Daruka Prasad B, Sharma SC, HemaPrabha P, *et al.* Multifunctional Dy (III) doped di-calcium silicate array for boosting display and forensic applications. J. Rare Earths. https://doi.org/10.1016/j.jre.2017.11.013.

10. Li BY, Zhang XL, Zhang LY, Wang TT, Li L, Wang CG, *et al.* NIR-responsive $NaYF_4:Yb,Er,Gd$ fluorescent upconversion nanorods for the highly sensitive detection of blood fingerprints. Dyes Pigm. 2016;134:178.

11. Sharma V, Das A, Kumar V, Ntwaeaborwa OM, Swart HC. Potential of $Sr_4Al_{14}O_{25}: Eu^{2+}, Dy^{3+}$ inorganic oxide-based nanophosphor in Latent fingermark detection. J Mater Sci. 2014;49:2225.

12. Jin Young Park, Hyun Kyoung Yang. Novel red-emitting $Y_4Zr_3O_{12}:Eu^{3+}$ nanophosphor for latent fingerprint technology. Dyes Pigm. 2017;141:348.

13. Darshan GP, Premkumar HB, Nagabhushana H, Sharma SC, Daruka Prasad B, Prashantha SC, *et al.* Superstructures of doped yttrium aluminates for luminescent and advanced forensic investigations. J Alloys Compd. 2016;686:577.

14. Dhanalakshmi M, Nagabhushana H, Sharma SC, Basavaraj RB, Darshan GP, Kavyashree D. Bio-template assisted solvothermal synthesis of broom-like $BaTiO_3:Nd^{3+}$ hierarchical architectures for display and forensic applications. Mater Res Bull. 2018;102:235.

15. Sandhyarani A, Kokila MK, Darshan GP, Basavaraj RB, Daruka Prasad B, Sharma SC, *et al.* Versatile core–shell $SiO_2@SrTiO_3:Eu^{3+},Li^+$ nanopowders as fluorescent label for

the visualization of latent fingerprints and anti-counterfeiting applications. Chem Eng J. 2017;327:1135.

16.   Xie HH, Wen Q, Huang H, Sun TY, Li PH, Li Y, *et al.* Synthesis of bright upconversionsubmicrocrystals for high-contrast imaging of latent-fingerprints with cyanoacrylate fuming. RSC Adv. 2015;5:79525.

17.   RajuGSR, Park J Y, Nagaraju GP, Pavitra E, Yang HK, Moon BK, *et al.* Evolution of $CaGd_2ZnO_5:Eu^{3+}$ nanostructures for rapid visualization of latent fingerprints. J Mater Chem C. 2017;5:4246.

18.   Dhanalakshmi M, Nagabhushana H, Darshan GP, Basavaraj RB, Daruka Prasad B. Sonochemically assisted hollow/solid $BaTiO_3:Dy^{3+}$ microspheres and their applications in effective detection of latent fingerprints and lip prints. J Sci Adv Mater Devices. 2017;2:22.

19.   Wang J, Ma QQ, Liu HY, Wang YQ, Shen HJ, Hu XX, *et al.* Time-gated imaging of latent fingerprints and specific visualization of protein secretions via molecular recognition. Anal Chem. 2017;89:12764.

20.   Wang M, Li M, Yang MY, Zhang XM, Yu AY, Zhu Y, *et al.* NIR-induced highly sensitive detection of latent fingermarks by $NaYF_4:Yb$, Erupconversion nanoparticles in a dry powder state. Nano Res. 2015;8: 1800.

21.   Cheng P, Deng CS, Gu MY, Dai XM. Effect of urea on the photoactivity of titania powder prepared by sol–gel method. Mater Chem Phys. 2008;107:77.

22.   Huang DG, Liao SJ, Liu JM, Dang Z, Petrik L. Preparation of visible-light responsive N–F-codoped TiO_2 photocatalyst by a sol–gel-solvothermal method. J Photochem Photobiol A, 2006; 184:282.

23.   Morikawa T, Irokawa Y, Ohwaki T. Enhanced photocatalytic activity of $TiO_2–xNx$ loaded with copper ions under visible light irradiation. Appl Catal A. 2006;314:123.

24.   Seery MK, George R, Floris P, Pillai SC. Silver doped titanium dioxide nanomaterials for enhanced visible light photocatalysis. J Photochem Photobiol A. 2007;189:258.

25.   Stengl V, Bakardjieva S. Molybdenum-doped anatase and its extraordinary photocatalytic activity in the degradation of orange II in the UV and vis regions. J Phys Chem C.2010;114:19308.

26.   Yang WG, Li JM, Wang YL, Zhu F, Shi WM, Wan FR, *et al.* A facile synthesis of anatase TiO_2 nanosheets-based hierarchical spheres with over 90% {001} facets for dye-sensitized solar cells. Chem Commun. 2011:47:1809.

27.   Xiang QJ, Yu JG, Wang WG, Jaroniec M. Nitrogen self-doped nanosized TiO_2 sheets with exposed {001} facets for enhanced visible-light photocatalytic activity. Chem Commun. 2011;47:6906.

28. Yang XH, Li Z, Liu G, Xing J, Sun CH, Yang HG, *et al.* Ultra-thin anatase TiO_2 nanosheets dominated with {001} facets: thickness-controlled synthesis, growth mechanism and water-splitting properties. Cryst Eng Comm.2011;13:1378.

29. Chen WP, Zhou AH, Yang X, Liu Y. Synthesis, structure and luminescence properties of $TiO_2:Eu^{3+}$ for white light-emitting diode. J Alloys Compd. 2013;581:330.

30. Salhi R, Deschanvres JL. Efficient green and red up-conversion emissions in Er/Yb co-doped TiO_2 nanopowders prepared by hydrothermal-assisted sol–gel process. J Lumin.2016;176:250.

31. Basavaraj RB, Nagabhushana H, Daruka Prasad B, Sharma SC, Venkatachalaiah KN, Mimosa pudica mediated praseodymium substituted calcium silicate nanostructures for white LED application. J Alloys Compd. 2017;690:730.

32. Craciun E, Predoana L, Atkinson I, Jitaru I, Anghel EM, Bratan V, *et al.* Fe^{3+}-doped TiO_2 nanopowders for photocatalytic mineralization of oxalic acid under solar light irradiation. J Photochem Photobio A Chem. 2018; 356:18.

33. Amith Yadav HJ, Eraiah B, Basavaraj RB, Nagabhushana H, Darshan GP, Sharma SC,*et al.* Rapid synthesis of C-dot@TiO_2 core-shell composite labeling agent: Probing of complex fingerprints recovery in fresh water. J Alloys Compd. 2018;742:1006.

34. Yogananda HS, Nagabhushana H, Darshan GP, Basavaraj RB, Daruka Prasad B, Sateesh MK, *et al.* MoO_3 nanostructures from EGCG assisted sonochemical route: Evaluation of its application towards forensic and photocatalysis. J Alloys Compd. 2018;745:874.

35. Suresh C, Nagabhushana H, Basavaraj RB, Darshan GP, Kavyashree D, Daruka Prasad B, *et al.* SiO_2@$LaOF:Eu^{3+}$ core-shell functional nanomaterials for sensitive visualization of latent fingerprints and WLED applications. J Colloid Interface Sci. 2018;518:200.

36. Toshiaki Ohsaka, Fujio Izumi, Yoshinori Fujiki. Raman spectrum of anatase, TiO_2. J Raman Spectrosc.1978;7:321.

37. Chaves A, Katiyan KS, Porto SPS.Coupled modes with A_1 symmetry in tetragonal $BaTiO_3$. Phys Rev B. 1974;10:3522.

38. Frank O, Zukalova M, Laskova B, Kurti J, Koltai J, Kavan L.Raman spectra of titanium dioxide (anatase, rutile) with identified oxygen isotopes (16, 17, 18). Chem Chem Phys. 2012;14:14567.

39. Basavaraj RB, Nagabhushana H, Daruka Prasad B, Sharma SC, Prashantha SC, Nagabhushana BM.A single host white light emitting $Zn_2SiO_4: Re^{3+}$ (Eu, Dy, Sm) phosphor for LED applications. Optik. 2015;126:1745.

40. Shivram M, Prashantha SC, Nagabhushana H, Sharma SC, Thyagarajan K, Harikrishna R, *et al.* $CaTiO_3:Eu^{3+}$ red nanophosphor: Low temperature synthesis and

photoluminescence properties. Spectrochim. Acta Part A Mol Biomol. Spec 2014;120:395.

41. Venkataravanappa M, Nagabhushana H, Daruka Prasad B, Darshan GP, Basavaraj RB, Vijayakumar GR.Dual color emitting Eu doped strontium orthosilicate phosphors synthesized by bio-template assisted ultrasound for solid state lightning and display applications. Ultrason Sonochem. 2017;34:803.

42. Renuka L, Anantharaju KS, Vidya YS, Nagaswarupa HP, Prashantha SC, Sharma SC, *et al.*A simple combustion method for the synthesis of multi-functional ZrO_2/CuO nanocomposites: Excellent performance as Sunlight photocatalysts and enhanced latent fingerprint detection. App Cata B Environ.2017;210:97.

43. Sodhi GS, Kaur J. Powder method for detecting latent fingerprints: a review. Forensic Sci Int. 2001;120:172.

44. Dhanalakshmi M, Nagabhushana H, Basavaraj RB, Darshan GP, Daruka Prasad B. Surfactant-assisted $BaTiO_3:Eu^{3+}@SiO_2$ core–shell superstructures obtained by ultrasonication method: dormant fingerprint visualization and red component of white light-emitting diode applications. ACS Sustainable Chem Eng. 2018;6:5214.
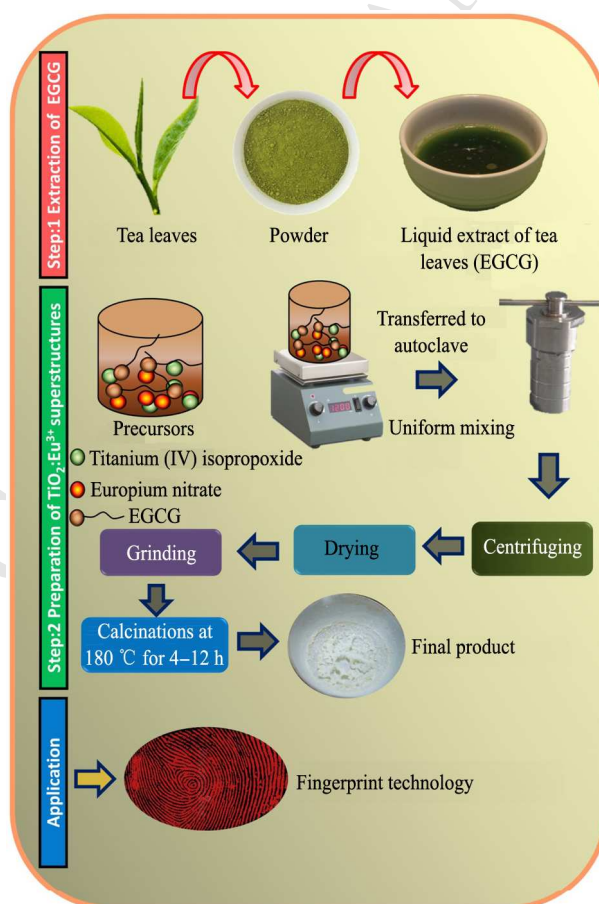
Fig.1. Schematic illustration for the hydrothermal synthesis of $TiO_2:Eu^{3+}$ NPs.
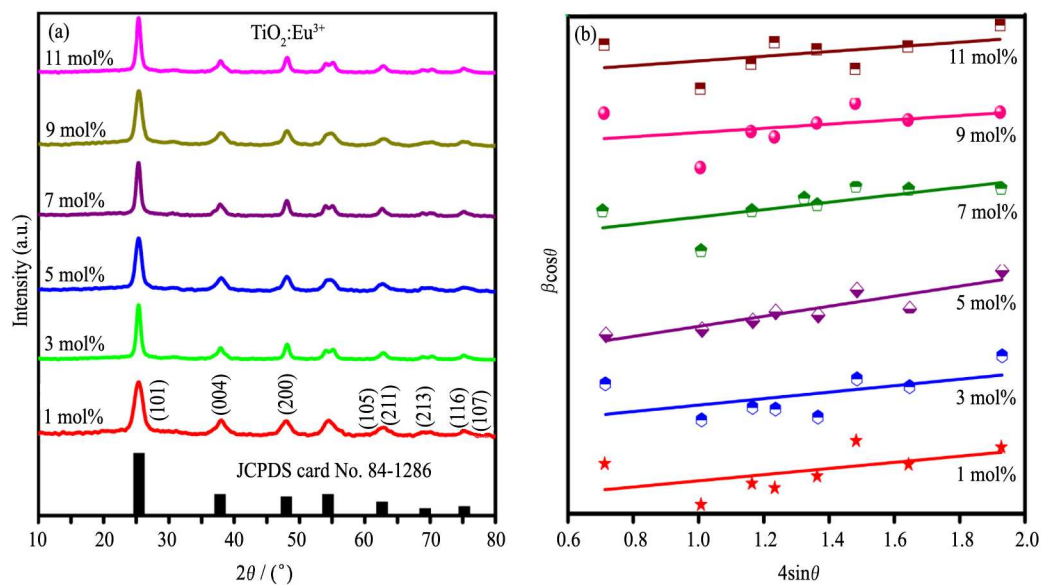
Fig. 2 PXRD patterns (a) and W-H plots (b) of TiO$_2$:Eu^{3+} (1 mol%–11 mol%) NPs.
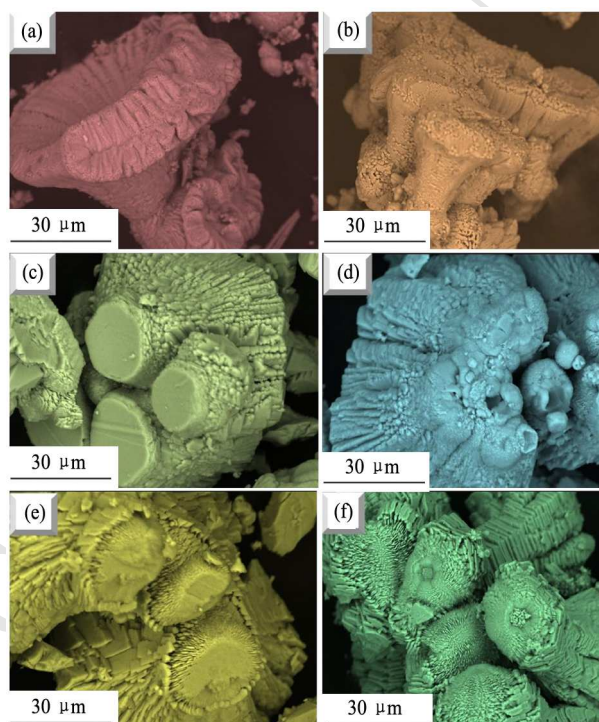
Fig.3.SEM micrographs of TiO$_2$:Eu^{3+} (5 mol%) NPs prepared by various concentrations of EGCG bio-surfactant. (a) 5 mL; (b) 10 mL; (c) 15 mL; (d) 20 mL; (e) 25 mL; (f) 30 mL
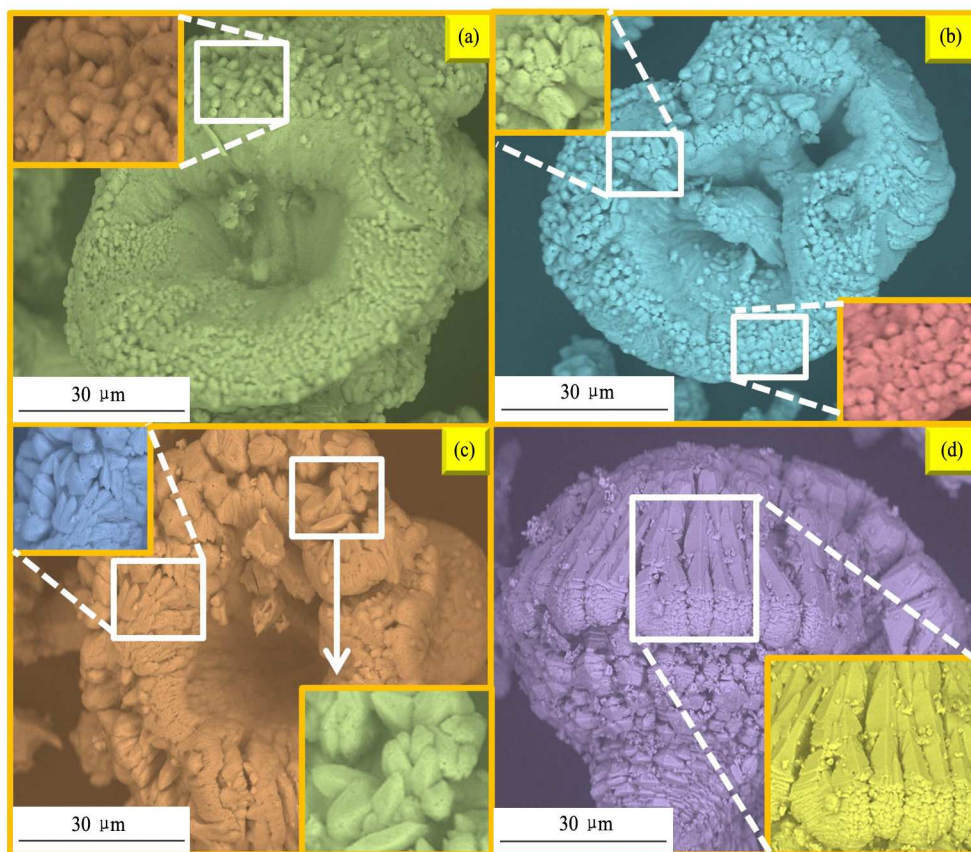
Fig.4. SEM images of TiO$_2$:Eu^{3+} (5 mol%) NPs prepared by different pH values of the solution 1 (a), 3 (b), 5 (c) and 9 (d) with fixed EGCG concentration (20 mL)
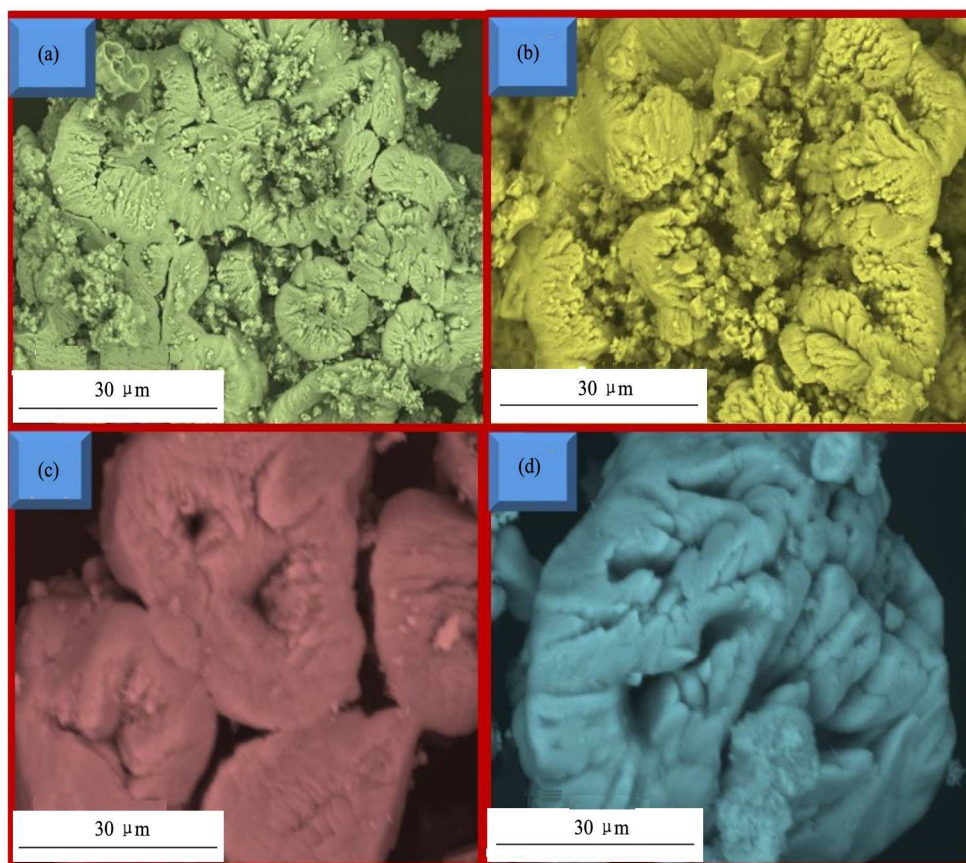
Fig.5. SEM images of TiO$_2$:Eu^{3+} (5 mol%) NPs prepared by different time period 6 h (a), 12 h (b), 18 h (c) and 24 h (d) with fixed EGCG concentration (20 mL) and pH =3.
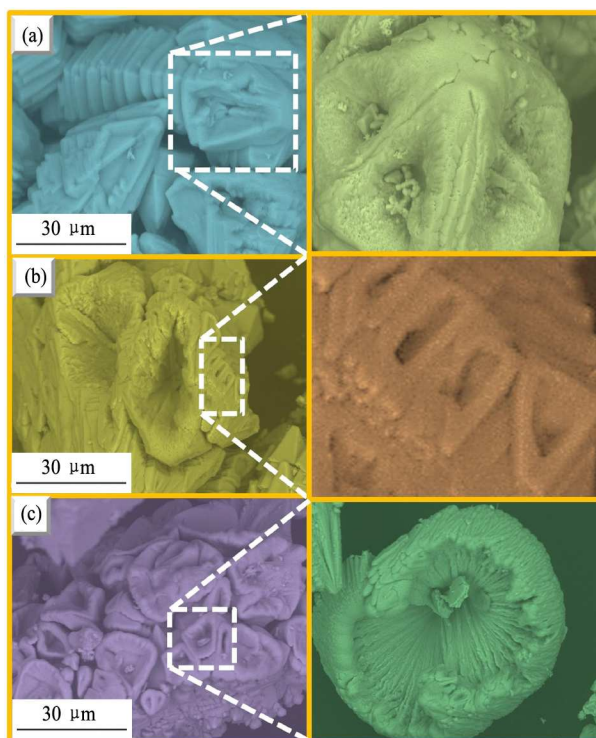
Fig.6. SEM images of TiO$_2$:Eu^{3+} (5 mol%) NPs prepared by various temperatures of 100 ^{o}C (a), 120 ^{o}C (b) and 140 ℃ (c) with fixed EGCG concentration (20 mL), pH 3 and time duration of 12 h.
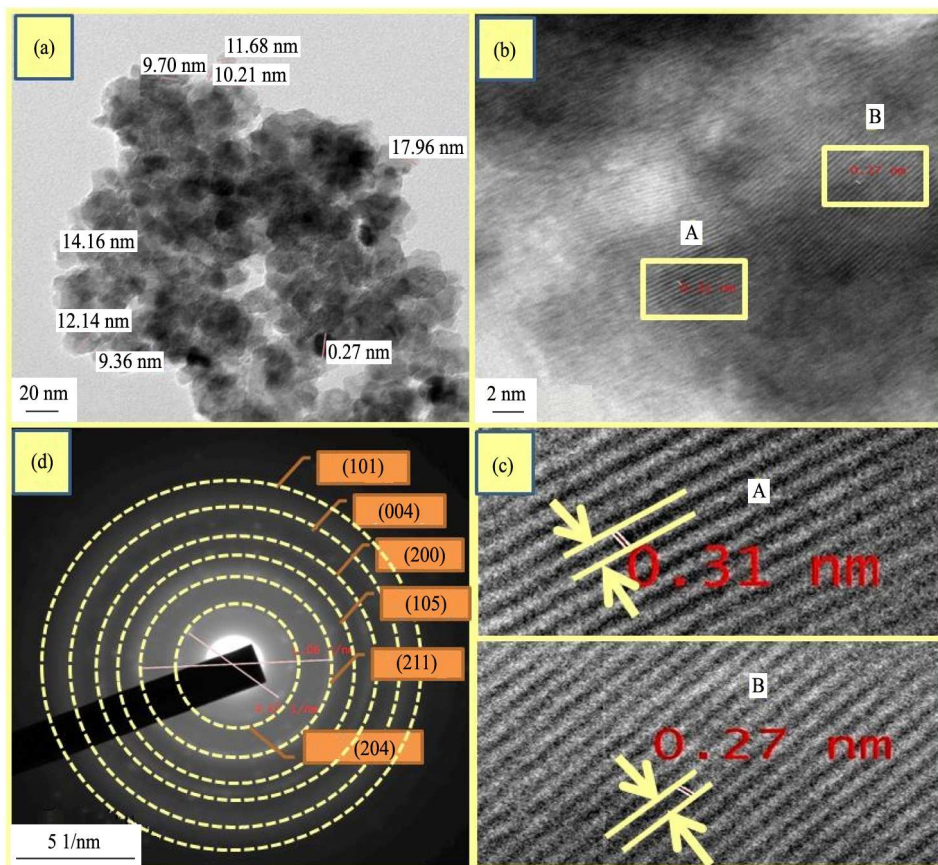
Fig. 7 TEM (a), HRTEM (b), and SAED (d) patterns of TiO$_2$:Eu^{3+} (5 mol%) NPs and enlarged view of HRTEM (c)
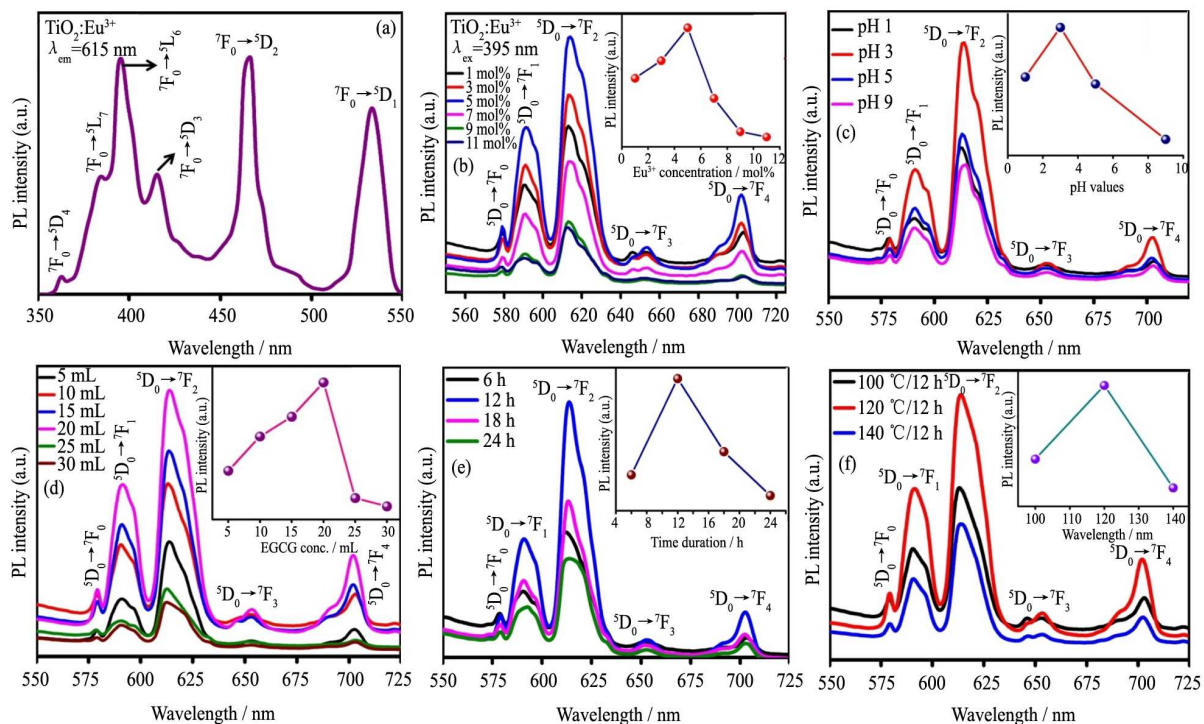
Fig.8 (a) PLE spectrum of TiO$_2$:Eu^{3+} (5 mol%) NPs, (b) emission spectra of TiO$_2$:Eu^{3+} (1 mol%–11 mol%) NPs and (c–f) emission spectra of samples prepared by various experimental conditions. Inset: variation of PL intensity with Eu^{3+} concentration, EGCG concentration, pH, time duration and reaction temperature.
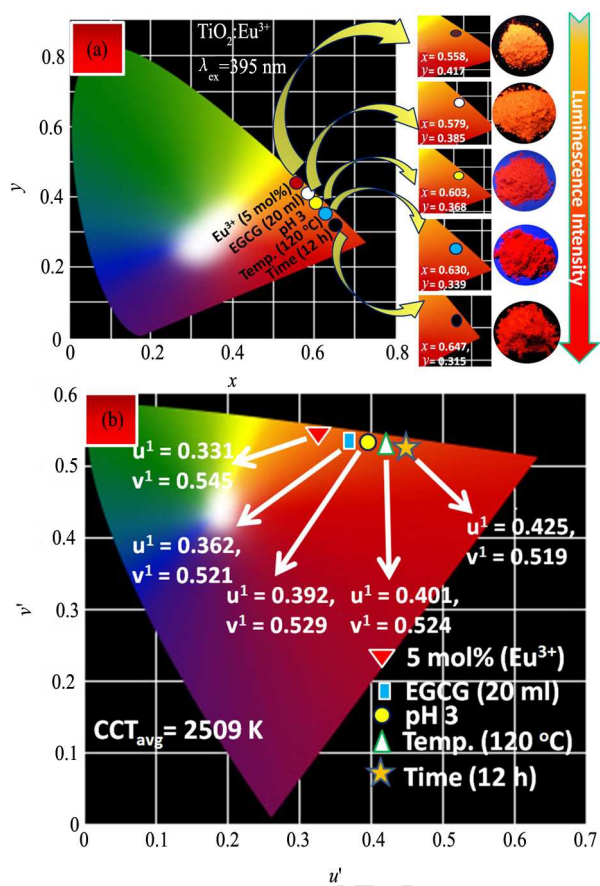
Fig. 9 CIE (a) and CCT (b) diagrams of optimized samples.
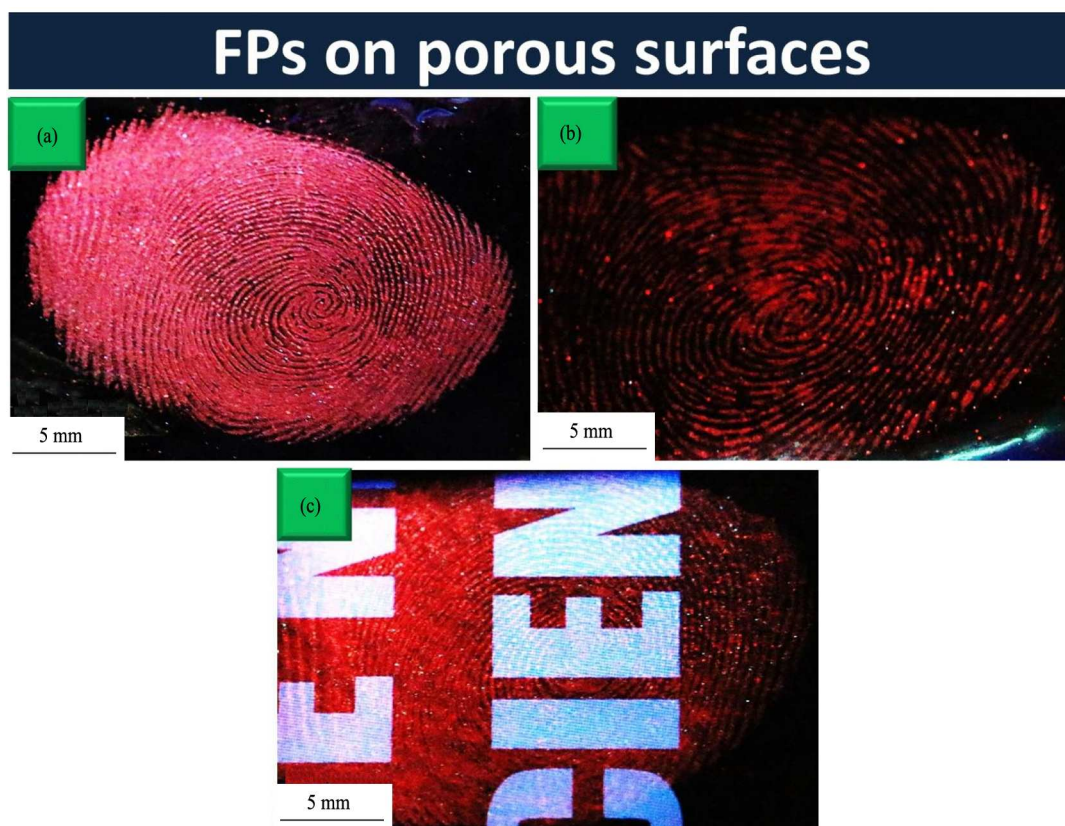
Fig.10. Visualized FPs by staining optimized TiO_2:Eu^{3+} (5 mol%) NPs on porous surfaces of (a) aluminum foil surface, (b) plastic sheet, (c) magazine cover under 254 nm UV light.
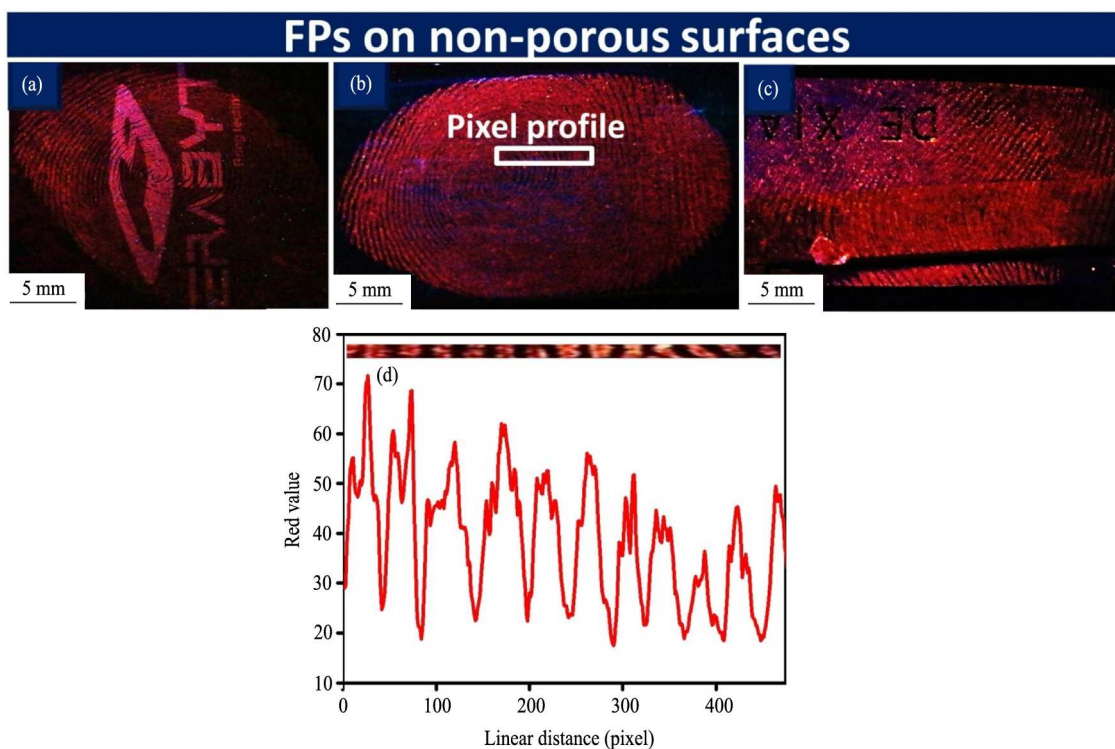
Fig.11 FPs visualized by using optimized $TiO_2:Eu^{3+}$ (5 mol%) NPs on various non-porous surfaces mouse (a), metallic scale (b), scissor (c) and pixel profile (d) showing the fluctuation of red value with ridges and furrows over a few papillary ridges indicated by rectangle box shown in Fig. 3(b).
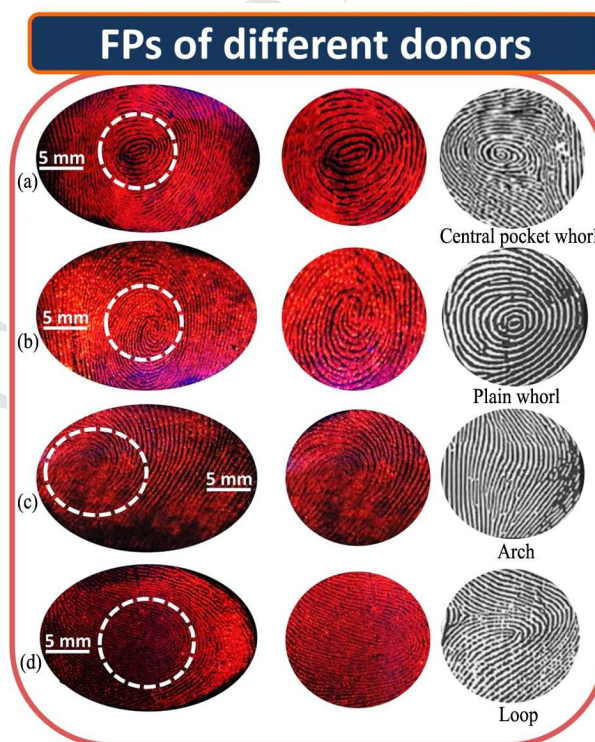

Fig.12. LFPs collected from various donors and visualized by staining $TiO_2:Eu^{3+}$ (5 mol%) NPs under 254 nm UV light followed by simple powder dusting technique.
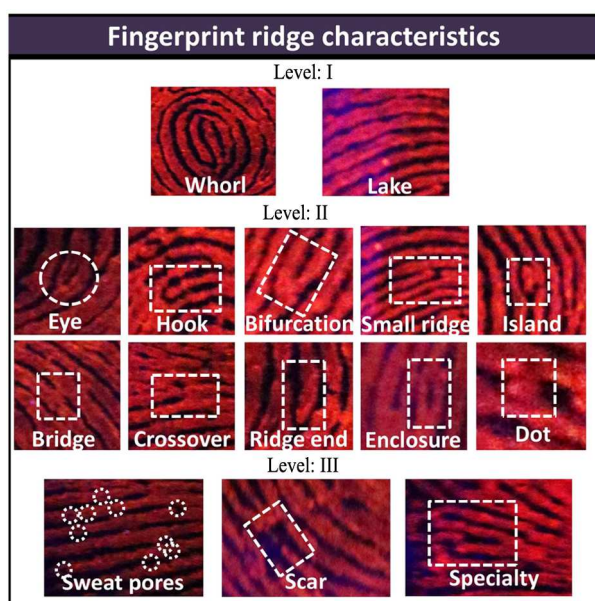
Fig.13. Visualized FPs using optimized NPs on aluminum foil surface showing various ridge details including level 1–3 under 254 nm UV light.
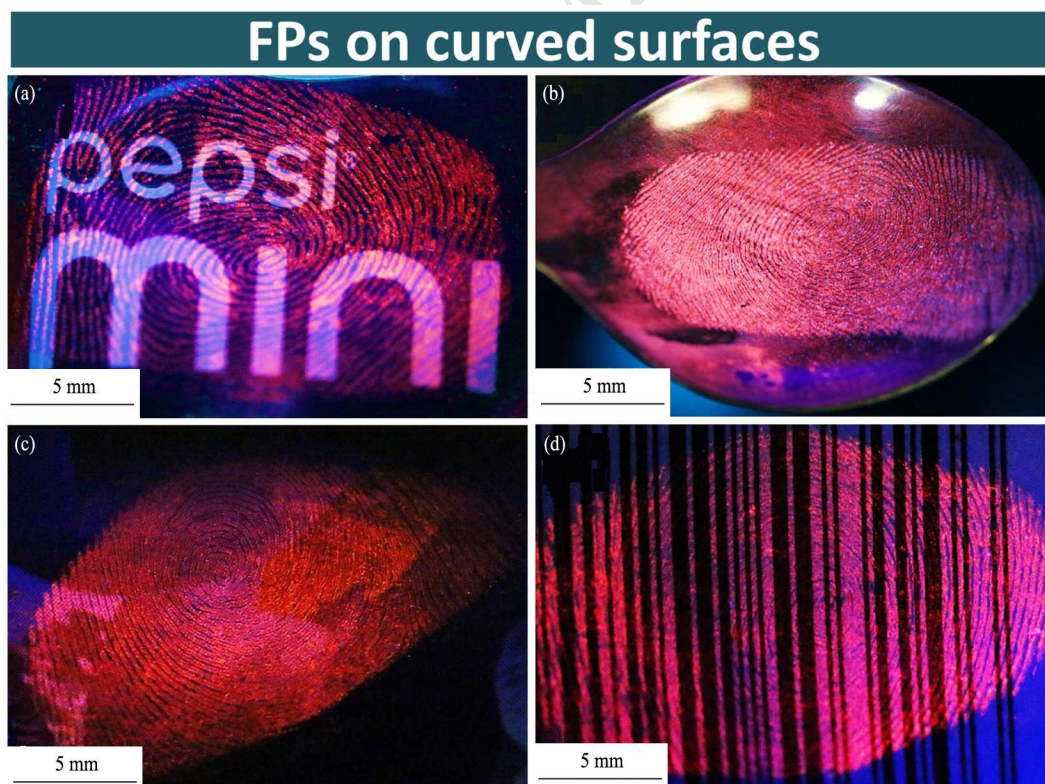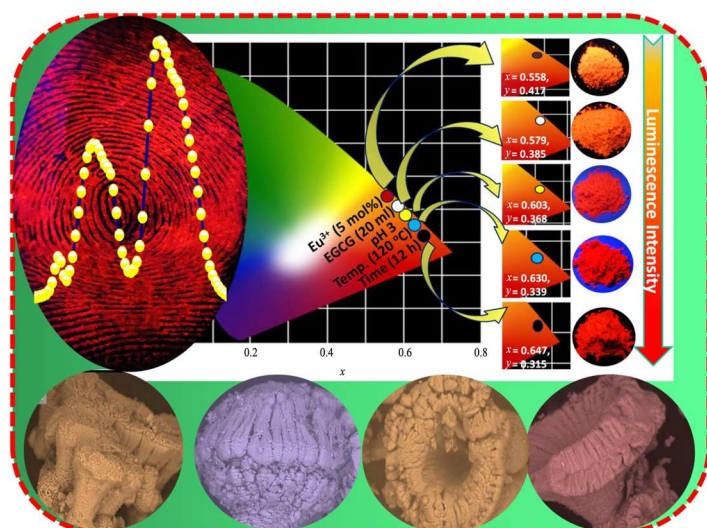

Fig.14. Visualized FPs on most neglected curved surfaces soft drink can (a), stainless steel spoon (b), spray bottle (c) and bar code (d) on chemical bottle under 254 nm UV light.

Table.1. Estimated crystallite size and strain values of Eu^{3+} (1 mol%–11 mol%) doped TiO_2 NPs.

Eu^{3+} (mol %)	Crystallite size (nm)		Strain $\mathring{a}$ ($\times 10^{-3}$)
	Scherrer's	W-H	
1	32	38	1.03
3	30	41	1.12
5	29	32	1.14
7	26	30	1.26
9	25	24	1.35
11	21	20	1.47

Eu^{3+} doped TiO_2 NPs were fabricated by hydrothermal route using EGCG as a biosurfactant. The optimized NPs could be used as authentication tool to visualization of latent fingerprints. The visualized fingerprints revealing clearly the third-level details (ridges, bifurcations and pores) with high selectivity, high contrast and no background interference.

Research Highlights

1. Eu^{3+} doped TiO_2 NPs were fabricated by hydrothermal route using EGCG as a bio-surfactant.

2. The optimized NPs could be used as authentication tool to visualization of latent fingerprints.

3. The visualized fingerprints revealing clearly the third-level details (ridges, bifurcations and pores) with high selectivity, high contrast and no background interference.